PCCP

PAPER

View Article Online
View Journal | View Issue

Cite this: *Phys. Chem. Chem. Phys.*, 2014, **16**, 4329

The pressure effect on thermotropic cubic phases of 1,2-bis(4′-*n*-alkoxybenzoyl)hydrazines†

Yoji Maeda,[a] Shoichi Kutsumizu*[b] and Shinichi Sakurai[c]

Received 22nd October 2013,
Accepted 7th December 2013

DOI: 10.1039/c3cp54471k

www.rsc.org/pccp

The effect of pressure on the nanostructure of a thermotropic cubic (Cub) mesogen 1,2-bis(4′-*n*-alkoxybenzoyl)hydrazine (BABH-*n*; *n* is the number of carbon atoms in the alkyl chain) was investigated under elevated pressures up to 140 MPa by an X-ray diffraction (XRD) technique. Four compounds, BABH-12, -14, -16 and -18, were examined and the type of Cub mesophase formed at ambient pressure is *Ia*3*d* for BABH-12 and -18, *Im*3*m* for BABH-14, and both for BABH-16. The high-pressure XRD enabled the discrimination of the Cub phase type in the low-pressure Cub phase regions of BABH-14 and BABH-16 and the revision of the phase diagrams reported previously. New insight in this work is changes in the lattice constant *a* of the Cub phases upon pressurization. The lattice constant *a* of the *Im*3*m*-Cub phase in BABH-14 decreases as only an exception, while those of the *Ia*3*d*-Cub phases in BABH-16 and -18 increased gradually, with increasing pressure, up to about 24 and 25% in the unit cell volume, respectively, in their optimal situations of pressure and temperature. The *a* values of the *Ia*3*d*-Cub phases in BABH-12, -14, -16 and -18 at elevated pressures were roughly on an extrapolated line of the *a* *vs.* *n* linear relationship determined for the corresponding data of the short-chain BABH-*n* ($6 \leq n \leq 13$) at ambient pressure. The pressure-induced expansion of the *Ia*3*d*-Cub lattice is well explained by reduced lateral expansion of a terminal alkyl chain and apparent reduction of the effective core size (from "double-layered core" to the "single-layered core" states).

1. Introduction

Thermotropic cubic (Cub) mesophases, especially bicontinuous types, have attracted great attention not only in the field of liquid crystals (LCs) but in a more broad area of soft matter. They possess both liquid-like molecular state and three-dimensional long-range periodicity in their aggregation structures.[1,2] The most often observed structure has a cubic symmetry $Ia\bar{3}d$, which consists of two pairs of 3-by-3 interpenetrating networks.[1a] Qualitatively, the formation of the $Ia\bar{3}d$-Cub phase is understood as a result of microphase separation between (at least) two chemically incompatible parts (*e.g.*, hydrophilic *vs.* hydrophobic or aliphatic *vs.* aromatic) and of packing frustration arising from the average molecular shape of constituent molecules.[1e,1f] Such understanding basically comes from the analogy of lyotropic Cub systems,[2] where the structures are related to triply periodic minimal surfaces (TPMS);[1d,2c] these curved surfaces are favored over parallel surfaces of lamellar phases when the volume ratio of the two components is deviated from 1 : 1. In thermotropic systems, however, it is not easy to predict precisely the stability of thermotropic Cub LC phases only from the chemical structure at present.[1j,k]

To date, many examples exhibiting thermotropic Cub phases have been accumulated such as carboxylic acids, hydrazines, chiral pyrimidine, lipids, metal mesogens, polyols, siloxanes, biforked mesogens, coil–rod–coil molecules, ionic polymers, ammonium salts, ionic triphenylene derivatives, and so on.[1] However, these synthetic efforts were not always followed by systematic surveys with respect to the chemical structure, and our knowledge is still very fragmented. The situation is in contrast to that in lyotropic Cub phases where several theoretical parameters are known to explain well the phase behaviors. To understand the formation mechanism of thermotropic Cub phases in terms of the chemical structure, it is important to investigate how each chemical part within the molecule contributes to the Cub phase formation when temperature is changed. Our first selection for this purpose was the 4′-*n*-alkoxy-3′-nitrobiphenyl-4-carboxylic acid (ANBC-*n*; *n* is the number of

[a] *Department of Life Science and Sustainable Chemistry, Faculty of Engineering, Tokyo Polytechnic University, 1583 Iiyama, Atsugi, Kanagawa 243-0297, Japan*
[b] *Department of Chemistry and Biomolecular Science, Faculty of Engineering, Gifu University, 1-1 Yanagido, Gifu 501-1193, Japan. E-mail: kutsu@gifu-u.ac.jp; Fax: +81-58-293-2794*
[c] *Department of Macromolecular Science and Engineering, Graduate School of Science and Technology, Kyoto Institute of Technology, Matsugasaki, Sakyo-ku, Kyoto 606-8585, Japan*

† Electronic supplementary information (ESI) available: Detailed phase behaviors of BABH-12, -14, -16, and -18 under pressures as viewed by XRD measurements (Fig. S1–S5 and S7–S10), *T*–*P* phase diagrams of BABH-8, -10 and -12 (Fig. S6) and an example of plausible snapshots for two hydrogen bonding fashions (Fig. S11). See DOI: 10.1039/c3cp54471k

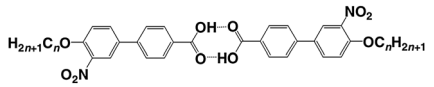

ANBC-*n*

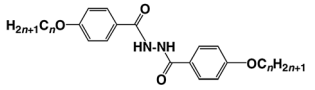

BABH-*n*

Chart 1

carbon atoms in the alkyl chain) series[3–9] and the next was the 1,2-bis(4′-*n*-alkoxybenzoyl)hydrazine (BABH-*n*) series (Chart 1).[10–16] In fact, exploration of the Cub phase formation in the same series provided us more fruitful insights than expected.

One of the epoch-making findings in the ANBC-*n*[7–9] and BABH-*n*[13–16] series is the formation of two types of Cub phases with symmetries $Ia\bar{3}d$ and $Im\bar{3}m$ (hereafter both denoted simply *Ia*3*d* and *Im*3*m*, respectively), where a re-entrant phase sequence *Ia*3*d*–*Im*3*m*–*Ia*3*d* is visible upon increasing the chain length or *n*; in the case of BABH-*n*, two regions of the *Ia*3*d*-Cub phase ($5 \leq n \leq 13$ and $15 \leq n \leq 22$) are intercepted by the *Im*3*m*-Cub phase region, as shown in Fig. 1.[14] Furthermore, upon varying the temperature, BABH-14 shows only the *Im*3*m*-Cub phase between crystal (Cr) and isotropic liquid (I) states, whereas BABH-13, -15, and -16 exhibit both types. The thermotropic *Im*3*m* phase is not identical to the lyotropic *Im*3*m* phase, and the nanostructure of the thermotropic *Im*3*m* phase has been proposed and discussed by us[15,17,18] and Zeng *et al.*[19,20]

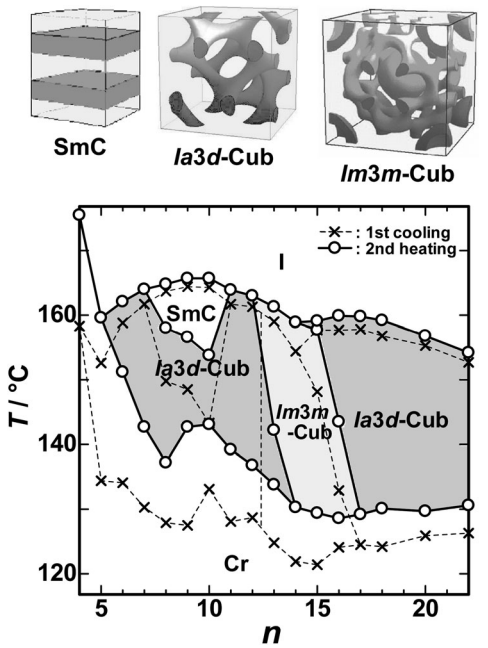

Fig. 1 (top) Schematic illustrations of nanostructures of SmC, *Ia*3*d*-Cub and *Im*3*m*-Cub phases and (bottom) transition temperature *vs. n* (number of carbon atoms in the alkyl chain) diagram for BABH-*n* homologues at ambient pressure.[14]

The second interesting feature is that BABH-8, -9, and -10 show an uncommon phase sequence Cr–*Ia*3*d*-Cub–SmC–I upon varying the temperature at ambient pressure,[11] because ANBC-*n* and many other cubic mesogens exhibit Cr–SmC–*Ia*3*d*-Cub (or *Im*3*m*-Cub)–I.[1c,4–8,21,22] Understanding of what parameters contribute to the free energy of the cubic mesophases, as a function of pressure as well as temperature, is very important for the complete description of thermodynamic phase stability.[23–34]

Two of the authors studied the *T*–*P* phase diagrams of BABH-8, -10, -11 and -12[32] using a high-pressure differential thermal analyzer and a polarized optical microscope (POM) equipped with a high-pressure hot stage. Triple points were found in the phase diagram of BABH-8 and -10 at which the Cr, *Ia*3*d*-Cub, and SmC phases coexist; the *Ia*3*d*-Cub–SmC transition line exhibits a negative slope with pressure ($dT/dP < 0$). On the other hand, BABH-11 and -12 were found to exhibit a pressure-induced SmC phase (SmC(hp)) at relatively low pressures and the slope of the SmC(hp)–*Ia*3*d*-Cub transition line is in both cases positive with pressure. In the intermediate pressure region, the phase sequence observed is Cr–SmC(hp)–*Ia*3*d*-Cub–I, a familiar order on the phase sequence for Cub phase forming compounds. Thus, according to the POM results, the inversion of the *Ia*3*d*-Cub and SmC phases in the phase sequence seems to occur at around $n = 11$.[33] Furthermore, a preliminary X-ray diffraction (XRD) experiment on BABH-14 revealed a pressure-induced reversible transition between the *Im*3*m*- and *Ia*3*d*-Cub phases by using isothermal pressure cycles at mesophase temperatures.[34] These findings urged us to investigate systematically the structural behavior of the Cub phases for BABH-12, -14, -16, and -18 homologues under hydrostatic pressures. The aim of this study is the completion of their *T*–*P* phase diagrams and clarification of the effects of both temperature and pressure on the mesophase nanostructures of BABH-*n* systems.

2. Experimental section

2.1 Materials

BABH-12, -14, -16, and -18 used in this study were prepared as described elsewhere.[10,14]

2.2 Measurements

Wide-angle XRD measurements under pressure were performed using a Bruker AXS Inc. ''D8 Discover'' wide-angle X-ray apparatus equipped with a ''Hi-Star'' two-dimensional position-sensitive proportional counter (PSPC). A high-pressure sample vessel was placed at the center of a wide-angle goniometer, in which the vessel was connected to a manually controllable oil-pump through a high-pressure tube. Silicone oil of low viscosity (10 centistokes), TSF 451-10, Toshiba Silicone Co., was used as the pressure medium. The silicone oil was pressurized up to about 140 MPa and supplied to the sample in the pressure vessel. A double cone type beryllium (Be) spindle, 6 mm o.d. in the central portion and 16 mm long, was used as the sample container, which has a vertical inner well of 1.2 mm i.d. for sample insertion. The powder sample was inserted into the well

of the Be spindle and then covered with epoxy adhesive, in order to fix the sample in the well and also to prevent the direct contact with the silicone oil. The Be spindle was set between the top and bottom heater blocks of the pressure vessel and then compressed for mechanical sealing of pressurized silicone oil. The temperature was measured using a chromel–alumel thermocouple that was in contact with the Be spindle, and the pressure was monitored using a Manganin gauge with a precision of ±1 MPa. Cu Kα X-rays (wavelength λ = 0.15418 nm) were generated at 40 kV and 40 mA, and collimated and directed to the sample in the Be spindle using a crossed-Göbel mirror. The camera length between the sample and the PSPC detector was 249 mm and the time of acquisition for each pattern ranged from 2 to 3 min. The XRD patterns were stored successively in a data processor during heating and cooling runs at a scanning rate of *ca.* 1 °C min^{-1} under various pressures. The absolute value of the *d*-spacing obtained was checked using a standard material (α-stearic acid) at 300 K and at ambient pressure and the deviation from the literature values was confirmed to be as small as 0.01 nm. We focused our attention on the mesophase formation, and the BABH-*n* system forms two types of Cub phases (*Ia*3*d* and *Im*3*m*) and a SmC phase. The two Cub phases have different absences of diffractions and in principle distinguishable by the XRD patterns.[13–16] As another feature, in the *Ia*3*d* phase, the (211) and (220) reflections are usually most intensely observed whereas the (321) reflection is usually the most intensified one in the *Im*3*m* phase.[1e,7,8,13–15,17,19,20] Representative XRD patterns of BABH-12, -14, -16 and -18 under pressures are given in Fig. S1 in ESI,† and selected data of observed *d*-spacings as a function of temperature, on which the above diagrams are based, are compiled in Fig. S2–S5 in ESI.† The error of the *d*-spacing under pressures was estimated at 0.03 nm in most cases, but in the vicinity of the transition point where two neighboring phases coexist, tending to become larger; the origin is not instrumental but is due to the orientational state of polycrystalline domains inside the sample container.

3. Results and discussion

3.1 *T*–*P* phase diagrams of BABH-12, -14, -16, and -18

The *T*–*P* phase diagrams constructed for BABH-12, -14, -16, and -18 are presented in Fig. 2. The diagrams of BABH-8 and -10, together with that of BABH-12, all of which were reported previously,[32] are given in Fig. S6 in ESI.† We focus our attention on the mesophase formation.

In the diagram, the Cub phase occupies a larger region (including ambient pressure) when viewed from *n* = 12 to 18. On the other hand, the SmC(hp) phase exists at the higher pressure region and the Cub phase neighbored by the SmC(hp) phase is *Ia*3*d* type. These general trends are the same as reported previously.[32] The boundary line dividing the two phase regions, which differs slightly between the heating and cooling runs, is terminated by two triple points. They correspond to the lower and upper limits of pressure for the formation of the SmC(hp) and Cub phases, respectively; the upper limits of pressure for the Cub phase (on the heating run) were 26, 60, 93, and 123 MPa for BABH-12, -14, -16, and -18, respectively, about twice larger than the values reported previously.[32]

Taking the type of cubic mesophase formed into consideration, the phase behaviors of the four BABH compounds under pressure are summarized as follows: the phase behavior of BABH-12 is essentially the same as reported previously[32] except for the boundary pressures. In the case of BABH-14, on the other hand, the low-pressure Cub region is divided into two regions, the *Im*3*m*-Cub phase below *ca.* 17 MPa and the *Ia*3*d*-Cub phase between 18 and 41 MPa. Here, the use of the high-pressure XRD technique has enabled the discrimination and the revision of the phase diagram reported.[32]

The behavior of BABH-16 is complicated: in the low-pressure region up to *ca.* 54 MPa, both *Im*3*m*- and *Ia*3*d*-Cub phases are visible at lower and higher temperature sides, respectively. Beyond the pressure, the *Im*3*m* phase vanishes and instead the SmC(hp) appears at the low temperature side of the *Ia*3*d*-Cub phase, and above *ca.* 93 MPa only the SmC(hp) phase remains. Unlike other BABH compounds, around 54 MPa, the lower limit of pressure for the formation of the SmC(hp) phase, there seem to be two triple points; one would correspond to a point at which the *Im*3*m*- and *Ia*3*d*-Cub and SmC(hp) phases coexist, and the other for the coexistence of the *Im*3*m*-Cub, SmC(hp), and Cr phases, although experimentally observed was either the SmC(hp) or the *Im*3*m*-Cub phase.

The behavior of BABH-18 under pressure is also divided into three pressure regions; the low-pressure region below *ca.* 83 MPa for the formation of the *Ia*3*d*-Cub phase, the high-pressure region beyond 123 MPa for the formation of the SmC(hp) phase, and the intermediate-pressure region for both phases between 83 and *ca.* 123 MPa. A complicated situation encountered for BABH-18 is the possibility of the presence of a pressure-induced *Im*3*m*-Cub phase, especially upon cooling around 70 MPa. This was also suggested by a preliminary SAXS experiment at the SPring-8.[35] Furthermore, the coexistence of the *Im*3*m*- and *Ia*3*d*-Cub phases was observed upon heating at the same pressure region.[35] Unfortunately, we were unable to identify the two Cub phase regions precisely; however, at least, it is certain that the *Ia*3*d*-Cub region at around 70 to 80 MPa, especially the low temperature side of the region, includes the *Im*3*m* region.

Table 1 summarizes the data on the triple points and the slope d*T*/d*P* of the Cub–SmC/SmC(hp) transition line for all the BABH homologues studied.

3.2 Relationship in molar volume between SmC and Cub phases

To see how the layer spacing (L_{SmC}) of the SmC or the SmC(hp) phase depends on the alkyl chain length (*n*), the L_{SmC} values obtained at 160 °C are plotted *vs.* *n* in Fig. 3. All the data points are on a straight line, irrespective of the pressure each sample is subjected to (*i.e.*, at ambient pressure or under pressures). The straight line determined by using the least-squares fit is L_{SmC}/nm = 1.49 + 0.15*n*. This result allows us to treat both the SmC and SmC(hp) phases equivalently, without distinguishing their formation processes.

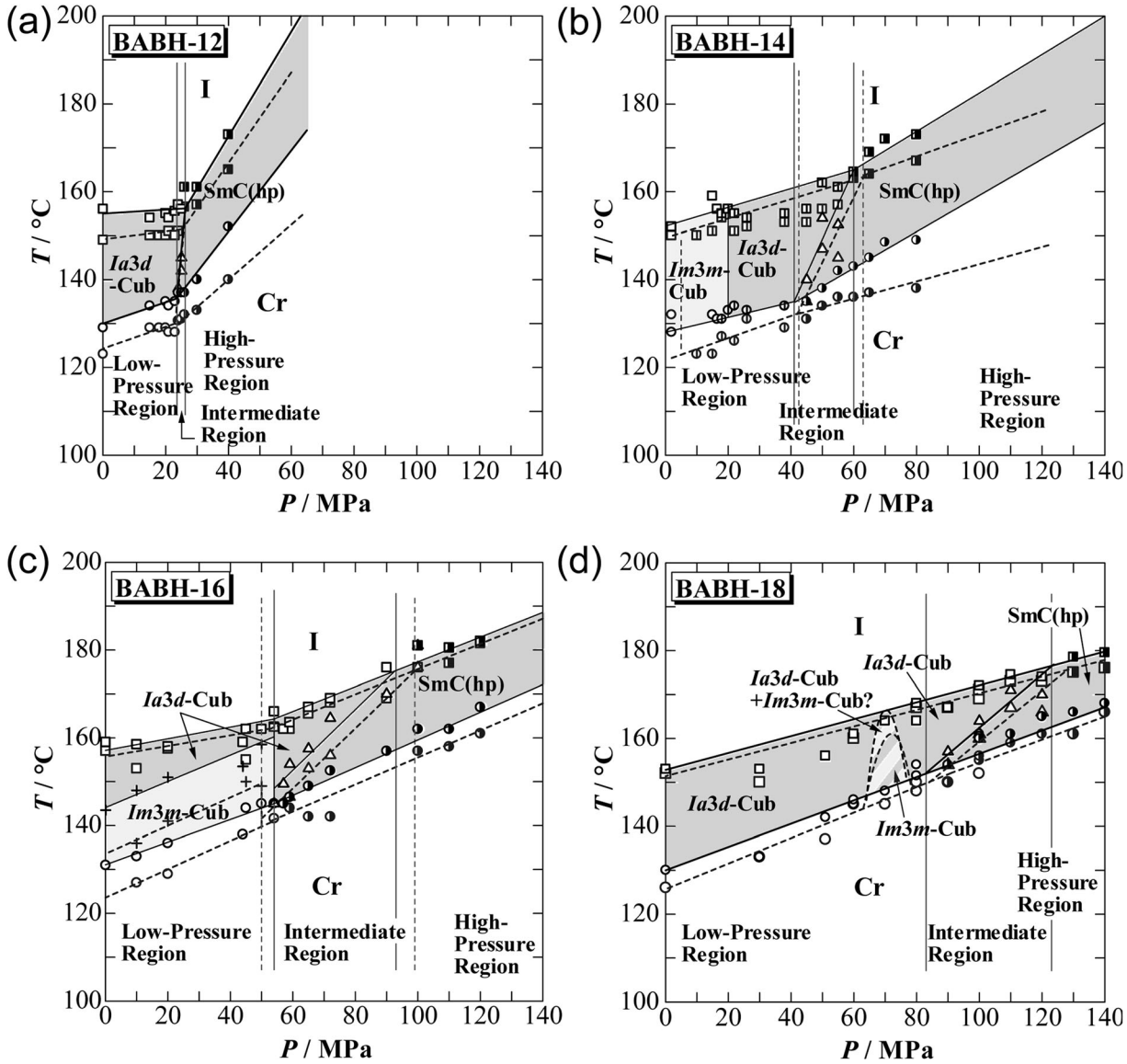

Fig. 2 *T*–*P* phase diagram of (a) BABH-12, (b) BABH-14, (c) BABH-16, and (b) BABH-18; solid and broken lines represent the boundaries upon heating and cooling, respectively; striped region in (d) indicates coexistence of *Ia3d* and *Im3m* phases upon heating (see the text).

Table 1 Triple points determined in the *T*–*P* phase diagrams of the homologous BABH-12, -14, -16, and -18 compounds

	Triple point (*T*/°C, *P*/MPa)					
BABH-*n*	$n = 8^a$	$n = 10^a$	$n = 12$	$n = 14$	$n = 16$	$n = 18$
Triple point 1 (upper limit of pressure for the Cub phase)	(≈140, 24)	(144, 10)	(156, 26)	(165, 60)	(175, 93)	(177, 123)
Triple point 2 (lower limit of pressure for the SmC phase)			(136, 24)	(135, 41)	—[b]	(152, 83)
Slope d*T*/d*P* (°C/MPa) of the Cub–SmC or the SmC–Cub transition line	−0.5	−1.0	+10	+1.6	+0.7	+0.6

[a] Ref. 32. [b] Not observed.

As mentioned in the earlier section, the Cub phase neighbored by the SmC phase is *Ia3d* type and the slopes of the *Ia3d*-Cub–SmC transition line are negative for BABH-8 and -10. In contrast, the corresponding slopes for BABH-12, -14, -16, and -18 are positive; d*T*/d*P* = +10, +1.6, +0.7, and +0.6 °C MPa^{-1}, respectively (Table 1). The change in the sign in d*T*/d*P* for the Cub–SmC transition line itself implies the inversion of the temperature location; for n = 8 and 10, the SmC phase is at the high temperature side of the *Ia3d*-Cub phase whereas the reverse is seen for $n \geq 12$. As discussed in our previous paper,[32]

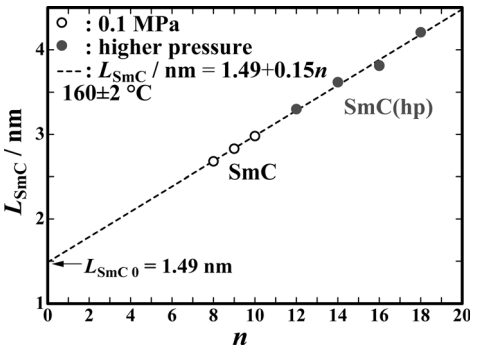

Fig. 3 Plot of the layer spacings (L_{SmC}) of the SmC (open circles) at ambient pressure and SmC(hp) (filled circles) phases under pressures against the alkyl chain length n.

the inversion is explained in the framework of a quasi-binary picture model proposed by Saito and Sorai.[18,36–38] Important points of their model are: (1) both systems are regarded as being composed of two molecular parts, the central core and alkyl chains at both ends and (2) when the system moves from the SmC to Cub phases the two parts would contribute to the transition entropy in different ways, unlike the usual phase transitions; at the transition the entropy of the chains increases while that of the remaining part, *i.e.*, the core part, decreases as a result of the formation of 3D network-like aggregations in the Cub phase. The total transition entropy is the sum of the two contributions, which is negative for n = 8–10 whereas positive for n > 12, reflecting their different chain lengths (Fig. S7 in ESI†). The fact that the phase sequence of Cr–SmC–Cub–I is observed not at the ambient pressure but under pressure (see Fig. 1 and 2) implies that not the entropy but the free energy governs the actual phase sequence realized, and also demonstrates the importance of the pressure studies.

The inversion also gives us the following relationship in molar volume between the SmC and *Ia3d*-Cub phases at the transition. In BABH-8 and -10, the transition enthalpy ΔH upon heating is positive at ambient pressure. In this case, applying the Clapeyron equation $dT/dP = \Delta V/\Delta S = T\Delta V/\Delta H$ to the transitions, negative ΔV ($= V_{SmC} - V_{Ia3d\text{-Cub}}$) is obtained. The resulting relationship of $V_{SmC} < V_{Ia3d\text{-Cub}}$ is unusual because the molar volume of the low-temperature *Ia3d*-Cub phase is larger than that of the high-temperature SmC phase. In a compound having a slightly longer chain, BABH-12, however, a normal trend of positive ΔV is obtained. Here, it should be noted that the common relationship $V_{Ia3d\text{-Cub}} > V_{SmC}$ at the Cub–SmC transition holds for all n irrespective of the inversion of the two phases in the temperature scale at n around 11.

3.3 Pressure dependence of *d* spacings of SmC(hp), *Ia3d*- and *Im3m*-Cub phases

Fig. 4 shows the pressure dependence of the d spacings of three mesophases. In BABH-12 at 145 °C (Fig. 4a), the (211) and (220) spacings of the *Ia3d*-Cub phase show almost no pressure dependence. On the other hand, the (001) spacing of the SmC(hp) phase decreases with increasing pressure. A small gap is visible between the *Ia3d*-Cub (211) and SmC(hp) (001) spacings at around 26 MPa. In BABH-14 at 145 °C (Fig. 4b), the two Cub phases show different pressure behaviors, a negative slope of the d spacings of the *Im3m*-Cub phase and a positive slope of the (211) and (220) spacings of the pressure-induced *Ia3d*-Cub phase, upon pressurization. At around 45 MPa, the *Ia3d*-Cub (211) spacing seems to be smoothly connected to the (001) spacing of the SmC(hp) phase, suggesting the epitaxial relationship between these two phases. Above about 50 MPa, the SmC(hp) (001) spacing shows a very subtle increase with pressure.

In BABH-16 at 150 °C (Fig. 4c), the *Ia3d*-Cub (211) and (220) spacings gently increase with increasing pressure up to about 50 MPa, with intermission of the *Im3m*-Cub phase region between 20 and 50 MPa, where the d spacings of the *Im3m*-Cub reflections are almost independent of pressure. At pressures between 50 and 60 MPa, very interestingly, the d spacings of the *Ia3d*-Cub phase jump up about 0.2 nm. At higher pressures above 60 MPa, the SmC(hp) (001) spacing decreases linearly with pressure. Fig. 4d shows the pressure behavior of BABH-18 at 150 and 160 °C. The *Ia3d*-Cub (211) and (220) spacings show a positive slope with pressure at both temperatures, whereas the slope of the SmC(hp) (001) spacing is negative.

3.4 Pressure dependence of the *Ia3d*- and *Im3m*-Cub lattices and the relationship in molar volume between the two Cub phases

On the basis of the pressure dependence of the d spacings mentioned above, we plot the lattice constant (a) of the two Cub phases for BABH-12, -14, -16, and -18 at selected temperatures as a function of pressure in Fig. 5. Here, note that the lattice constant corresponds to the nano-scale periodicity of molecular aggregations, and never implies the long-range ordering of each component molecule within the lattice. The value of $(1/a_0)(da/dP)$ for the *Im3m* phase ranges from -1.1×10^{-3} MPa^{-1} (BABH-14) to $+3.2 \times 10^{-4}$ MPa^{-1} (BABH-16) (a_0 is the lattice constant at a mid pressure in each phase region). The value for the *Ia3d* phase, on the other hand, varies from $+7.2 \times 10^{-5}$ MPa^{-1} (BABH-12) to $+4.3 \times 10^{-4}$ MPa^{-1} (BABH-16) and to $+8.3 \times 10^{-4}$ MPa^{-1} (BABH-18), and all positive. For lyotropic *Ia3d*-Cub phases, reported values (absolute values) range from 0.3 to 1.5×10^{-4} MPa^{-1},[29–31] which are positive for the inverse phases whereas negative for the normal phases. The fact suggests that our system corresponds to the inverse type. An interesting point is the corresponding values of pressure-induced *Ia3d* phases, which are $+2.5 \times 10^{-3}$ MPa^{-1} for BABH-14 and $+3.4 \times 10^{-3}$ MPa^{-1} for BABH-16, much larger than the values for the *Ia3d* phase formed at ambient pressure.

Table 2 summarizes the structural parameters of both *Ia3d*- and *Im3m*-Cub phases for BABH-n under pressure.

As for the phase boundary between the *Im3m*- and *Ia3d*-Cub phases, a linear equation $T/°C = 144.1 + 0.2994 \times (P/MPa)$ is obtained for BABH-16. Applying the Clapeyron equation to the transition line, a positive ΔV ($= V_{Ia3d} - V_{Im3m}$) is obtained and thus a relationship $V_{Ia3d} > V_{Im3m}$ is concluded because both the ΔH (heat of transition at ambient pressure) and dT/dP

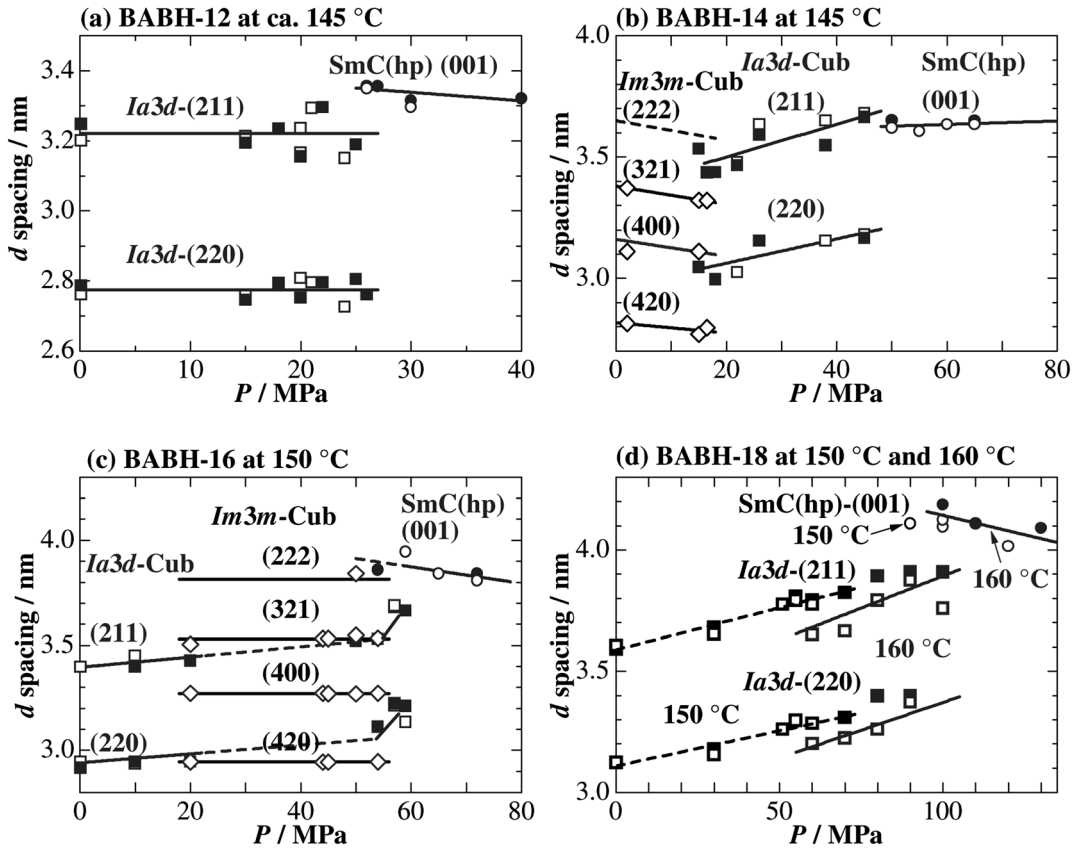

Fig. 4 *d* spacings of reflections of three mesophases against pressure for (a) BABH-12, (b) BABH-14, (c) BABH-16, and (d) BABH-18 at indicated temperatures; open and filled symbols represent the data obtained upon heating and cooling at each pressure, respectively.

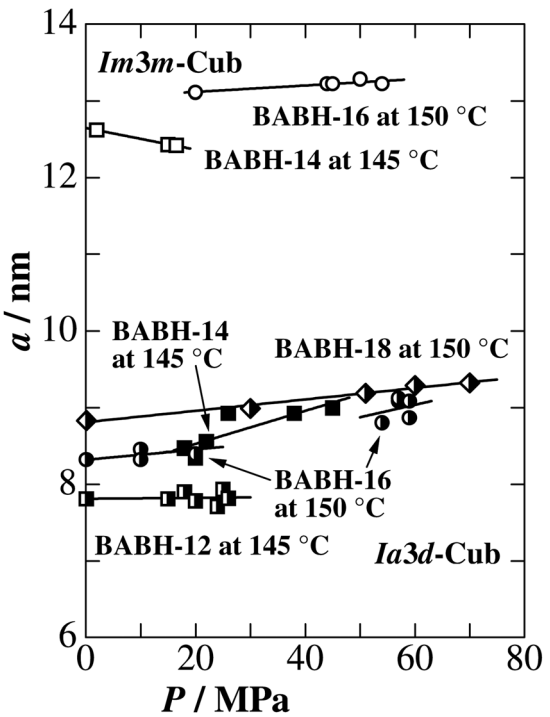

Fig. 5 Pressure dependence of the lattice constant (*a*) of the Cub phases for BABH-12 at 145 °C, BABH-14 at 145 °C, BABH-16 at 150 °C, and BABH-18 at 150 °C.

are positive. The positive ΔV is a normal transition behavior from the thermodynamic point of view. For BABH-14, on the other hand, the corresponding boundary rises almost perpendicular in the *T*–*P* phase diagram, suggesting that ΔS ($= S_{Ia3d\text{-Cub}} - S_{Im3m\text{-Cub}}$) is close to zero.

3.5 How does pressure affect the phase stability of the *Im3m* and *Ia3d* cubic phases?

In the previous publication,[14] one of the authors discussed how temperature affects the average molecular shape in connection with the formation of Cub phases in a certain temperature range for the BABH system. The molecular shape is mainly governed by two temperature-dependent factors: (i) intermolecular hydrogen bonds at the central core and (ii) lateral thermal expansion of the terminal alkyl chain at both molecular ends. If the terminal chain is in a nearly extended form, the molecular shape can be approximated to a rod, which is in favor of a layered structure such as in the SmC phase. Elevating the temperature, however, would enhance thermal motion of the terminal chains (*i.e.*, factor ii), changing the molecular shape from a rod to a two-megaphone-connected one, as schematically illustrated in Fig. 6a. The resulting tapered shape, if the hydrogen bonding is retained to hold the neighboring molecules close to each other against thermal disturbance, would cause fragmentation of the layer into small triangular pieces to

Table 2 Structural parameters of the *Ia3d*- and *Im3m*-Cub phases of BABH-*n* under pressure

				Lattice constant a and volume of unit lattice V							
	P = 0.1 (MPa)	T (°C)	Type	a (nm)	$V_{0.1}$ (nm^3)	P (MPa)	T (°C)	Type	a (nm)	V_P (nm^3)	$V_P/V_{0.1}$
BABH-12	0.1 MPa	146, heating	*Ia3d*	7.83	480	24	148, heating	*Ia3d*	7.82	478	≈1
BABH-14	2.0 MPa	146, heating	*Im3m*	12.55	1977						
						22	147, heating	*Ia3d*	8.54	623	
						38	146, heating	*Ia3d*	8.93	712	
						50	161, heating	*Ia3d*	8.39	591	
BABH-16	0.1 MPa	141, heating	*Im3m*	13.10	2248	50	149, heating	*Im3m*	13.22	2310	1.03
		152, heating	*Ia3d*	8.33	578	72	167, heating	*Ia3d*	8.96	719	1.24
BABH-18	0.1 MPa	153, heating	*Ia3d*	8.83	688	110	174, heating	*Ia3d*	9.52	863	1.25

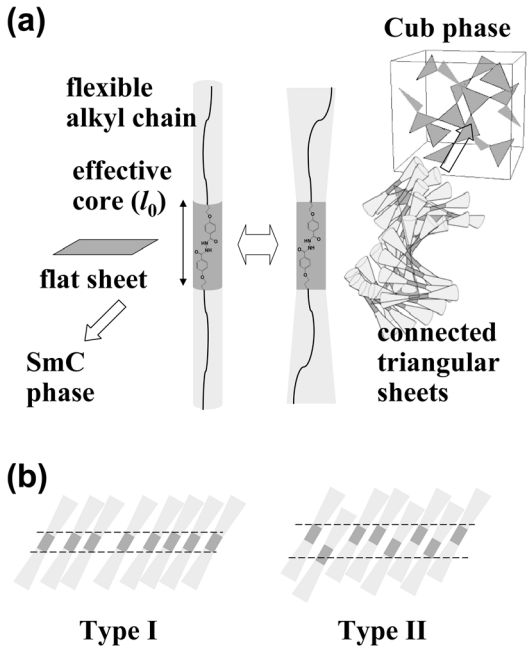

Fig. 6 (a) Schematic representations of a rod shape favoring a lamellar type SmC structure and a two-megaphone-connected one bringing about packing frustration within the lamellar structure, leading to connected triangles with a cubic symmetry,[16] and (b) two types of lateral packing modes (see the text for details).

relax packing frustration that would be accumulated within the lamellar SmC phase maintained. The resulting triangles are placed in harmony with a cubic symmetry, finally leading to the formation of a Cub phase.[16] On the other hand, if the hydrogen bonding becomes rather weakened (*i.e.*, factor i), neighboring central cores are able to take a longer separation between them to reduce the packing frustration, which would be allowed to maintain the SmC layered structure.

Application of pressure would affect the two factors in different ways: (a) by strengthening the intermolecular hydrogen bond between the core parts and (b) by reducing the lateral expansion of the terminal alkyl chain. The direction of each effect is the same when temperature is reduced. However, if the former effect is predominant, the extent of the tapered molecular shape is enhanced; reversely, the latter effect reduces the extent. The information on the change in the tapered extent is obtained by the change in the lattice constant of each Cub phase upon varying temperature or pressure. Under the isothermal conditions, for example, reduction of the extent with increasing pressure would require more molecules to build up a unit lattice of the Cub phase, leading to an increase in the lattice constant, whereas the reverse trend would lead to a decrease in it. It is, however, not realistic that application of pressure contributes to only one of the two factors. It would be more plausible to consider that the pressurization actually affects the two factors simultaneously at low pressures, apart from which is the major one, and as seen below, the reduction of the lateral expansion of alkyl chains would probably persist at higher pressures. In fact, only in the case of BABH-14 at low pressures, the predominant contribution of strengthening the hydrogen bond is suggested for the observed decrease in the lattice constant of the *Im3m* phase upon pressurization (see Fig. 4b and 5). For this phase, a decrease in the lattice constant was observed when temperature is elevated,[14] and pressurization and reducing temperature do not provide the same effect in this case. In other cases, an increase in the lattice constant of the Cub phase upon pressurization was observed (Fig. 5), suggesting that the major factor is the effect on the chain; and also simple correspondence of pressurization and reducing temperature is realized. In the SmC phase region, pressurization decreases the layer spacing in most cases (Fig. 4a, c, and d) whereas reducing the temperature reversely increases the spacing (Fig. S2c, S3d, S4b, and S5f, ESI†).

A previous publication[14] revealed that the lattice constant at ambient pressure shows good linear relationships with n in three regions; a/nm = 3.91 + 0.31n for the *Ia3d*-Cub phase of the BABHs with $6 \leq n \leq 13$ (denoted Type I), a/nm = 4.72 + 0.22n for the *Ia3d*-Cub phase of the BABHs with $15 \leq n \leq 22$ (denoted Type II), and a/nm = 6.91 + 0.38n for the *Im3m*-Cub phase of $13 \leq n \leq 16$. The three plots of a *vs.* n are shown in Fig. 7. The two *Ia3d* phase regions have different extrapolated a_0 values at $n = 0$; a_0 = 3.91 nm (in Type I) and 4.72 nm (Type II). Boldly speaking, the larger a_0 would correspond to larger effective core size (l_0 in Fig. 6a), where the effective core includes not only the aromatic core part but also some part of the chain with suppressed dynamics in the vicinity of the core.[14] Recent full structural analysis of the two *Ia3d* phases has

supported this speculation: in the long-chain BABH-*n*s, the electron density map indicates the presence of two maxima inside the core aggregation region, implying two clusters of the molecular cores in this region; this Type II packing mode, also called the ''double-layered core'', has a larger effective core size than the Type I packing mode called the ''single-layered core''. The situation is schematically illustrated in Fig. 6b. The presence of two effective core lengths is assigned to different types of hydrogen bonding fashions[16] and an example of plausible snapshots for them is presented in Fig. S8 in ESI.† It is worth noting that the Type II packing has not only a larger effective core size but also weaker interactions between the core parts, both of which would reduce the extent of the tapered shape and would be considered as a reason for the re-entrant formation of the *Ia*3*d* phase in the long-chain BABH-*n*s.

Returning to the pressure effect and plotting the data under pressure in the same plot in Fig. 7, one can see that the data for the *Im*3*m* phases are placed almost at the same positions of the corresponding data at ambient pressure. This is linked to a rather small sensitivity of the *Im*3*m* phase structure with pressure as we see in Fig. 5. On the other hand, the data points of the *Ia*3*d* phases of n = 16 and 18 show about 24% and 25% increase in the unit cell volume in their optimal situations of pressure and temperature, respectively, as compared with the ambient values (see Table 2), which are well situated on the straight line of a/nm = 3.91 + 0.31n for the short-chain *Ia*3*d* phase at ambient pressure. Considering that their ambient phases are in the ''double-layered core'' (Type II) state, it is suggested that application of pressure modifies the hydrogen bonding fashion in the *Ia*3*d* structure into the ''single-layered core'' (Type I) state. Interestingly, for the pressure-induced *Ia*3*d* phase of BABH-14, the initial data point at around 20 MPa is on the above-mentioned straight line, but the data rather deviate from it when the pressure is in a medium range such as 38 MPa. This phenomenon may be related to the fact that only at this chain length the *Ia*3*d* phase is not stabilized at ambient pressure, but the detailed origin is not certain.

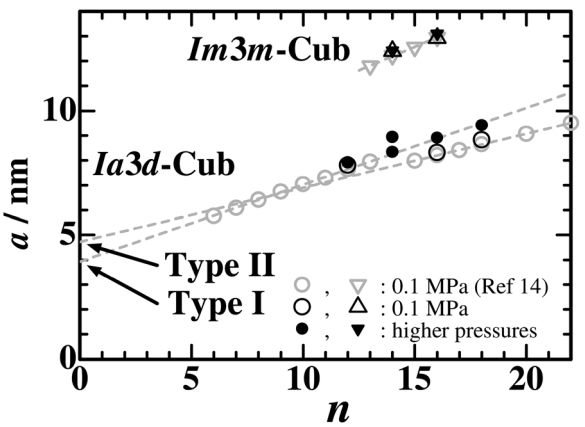

Fig. 7 Change in the lattice constant a of the *Ia*3*d*-Cub (circles) and *Im*3*m*-Cub (triangles) phases at ambient pressure and under pressures for n = 12, 14, 16, and 18, together with the data obtained from ref. 14 (grey symbols); two data points are plotted for the *Ia*3*d*-Cub phase of n =14 at 20 and 38 MPa (the upper one).

4. Conclusions

In this study, the *T*–*P* phase diagrams of the mesophases have been established for four Cub-phase forming compounds, BABH-12, -14, -16, and -18. In the diagrams, the Cub phase occupies a larger region (including ambient pressure) when viewed from n = 12 to 18. On the other hand, the SmC(hp) phase exists at a higher pressure region and it has been confirmed that the Cub phase neighbored by the SmC(hp) phase is *Ia*3*d* type. For BABH-14, the diagram has been revised and the low-pressure Cub region contains two regions, the *Im*3*m*-Cub phase below *ca.* 17 MPa and the *Ia*3*d*-Cub phase between 18 and 41 MPa. For BABH-16, it has been confirmed that both *Im*3*m*- and *Ia*3*d*-Cub phases are formed at lower and higher temperature sides, respectively, below *ca.* 54 MPa. Beyond the pressure, the *Im*3*m* phase vanishes and instead the SmC(hp) phase appears at the low temperature side of the *Ia*3*d*-Cub phase, and above *ca.* 93 MPa only the SmC(hp) phase remains. Here, the use of the high-pressure XRD technique has enabled the discrimination of the Cub phase type and the revision of the phase diagram reported.

A new insight in this work is changes in the lattice constant a of the Cub phases upon pressurization. In this regard, this work provides the first example of thermotropic Cub systems examined under pressures. In BABH-12, the increase was quite small, which is closely related to the fact that the SmC phase is induced at relatively low pressure (>26 MPa). In BABH-14, a decrease in the lattice constant of the *Im*3*m* phase was observed with increasing pressure as only an exception, and the pressure-induced *Ia*3*d*-Cub phase showed a large increase in the lattice constant with increasing pressure. This trend was most prominent for BABH-16 and -18, and the expansion finally reached *ca.* 24% and 25% in the unit lattice volume, respectively, in their optimal situations of pressure and temperature, compared with those at ambient pressure. These results are closely connected with an important feature of the Cub mesophase that the extent of the tapered shape of constituent molecules determines the periodicity of the phase, and except for the *Im*3*m* phase of n = 14 at low pressures, the major factor of applying pressure was the effect on the terminal alkyl chain.

Another finding is that the a values of the *Ia*3*d*-Cub phase of BABH-12, -14, -16, and -18 at elevated pressures are roughly on the extrapolated line of the a *vs.* n linear relationship for the *Ia*3*d*-Cub phase of the short-chain BABHs with $6 \leq n \leq 13$ at ambient pressure. This strongly suggests that application of pressure induces a change in molecular aggregation from the ''double-layered core'' (Type II) to the ''single-layered core'' (Type I) states. In contrast, the pressure-sensitivity of the *Im*3*m*-Cub lattice of BABH-14 and -16 was quite small. It is most probable that the *Im*3*m*-Cub phase is stabilized with a delicate balance of the hydrogen bonding and alkyl chain states.

Acknowledgements

The authors thank Dr Hiroyuki Mori for the preparation of the samples used in this study and Prof. Kazuya Saito at the University of Tsukuba for his valuable comments on the *Ia3d*- and *Im3m*-Cub structures. The authors also thank Mr Ryo Hori for his aid in making an illustration. SK is grateful for financial support from the Ministry of Education, Culture, Sports, Science, and Technology, Japan [Grant-in-Aid for Scientific Research on Priority Area "Super-Hierarchical Structures" (No. 446/19022012)] and from the Japan Society for the Promotion of Science (Grant-in-Aid for Scientific Research (C) 18550121 and (C) 25410091). SS acknowledges the SPring-8 facilities for the SAXS measurements under pressure (2005B0383, 2009A1153 and 2010A1121).

References

1 (*a*) V. Luzzati and P. A. Spegt, *Nature*, 1967, **215**, 701–704; (*b*) A. Tardieu and J. Billard, *J. Phys. Colloq.*, 1976, **C3**(37), 79–81; (*c*) G. W. Gray and J. W. Goodby, *Smectic Liquid Crystals*, *Textures and Structure*, Leonard Hill Glasgow, 1984, pp. 68–81; (*d*) S. Diele and P. Göring, in *Handbook of Liquid Crystals*, ed. D. Demus, J. Goodby, G. W. Gray, H.-W. Spiess and V. Vill, Wiley-VCH Weinheim, 1998, vol. 2B, pp. 887–900; (*e*) A.-M. Levelut and M. Clerc, *Liq. Cryst.*, 1998, **24**, 105–115; (*f*) C. Tschierske, *Annu. Rep. Prog. Chem., Sect. C: Phys. Chem.*, 2001, **97**, 191–267; (*g*) S. Diele, *Curr. Opin. Colloid Interface Sci.*, 2002, **7**, 333–342; (*h*) S. Kutsumizu, *Curr. Opin. Solid State Mater. Sci.*, 2002, **6**, 537–543; (*i*) M. Impéror-Clerc, *Curr. Opin. Colloid Interface Sci.*, 2005, **9**, 370–376; (*j*) M. Yoneya, *Chem. Rec.*, 2011, **11**, 66–76; (*k*) S. Kutsumizu, *Isr. J. Chem.*, 2012, **52**, 844–853.

2 (*a*) P. Mariani, V. Luzzati and H. Delacroix, *J. Mol. Biol.*, 1988, **204**, 165–189; (*b*) J. M. Seddon and R. H. Templer, *Philos. Trans. R. Soc. London*, 1993, **344A**, 377–401; (*c*) S. Hyde, S. Andersson, K. Larsson, Z. Blum, T. Landh, S. Lidin and B. W. Ninham, *The Language of Shape, The Role of Curvature in Condensed Matter: Physics, Chemistry and Biology*, Elsevier Amsterdam, 1997; (*d*) *Bicontinuous Liquid Crystals: Surfactant Science Series*, ed. M. L. Lynch and P. T. Spicer, CRC Press Boca Raton, FL, 2005, vol. 127.

3 G. W. Gray, B. Jones and F. Marson, *J. Chem. Soc.*, 1957, 393–401.

4 D. Demus, G. Kunicke, J. Neelsen and H. Sackmann, *Z. Naturforsch., A: Phys. Sci.*, 1968, **23**, 84–90.

5 D. Demus, D. Marzotko, N. K. Sharma and A. Wiegeleben, *Krist. Tech.*, 1980, **15**, 331–339.

6 S. Kutsumizu, M. Yamada and S. Yano, *Liq. Cryst.*, 1994, **16**, 1109–1113.

7 S. Kutsumizu, T. Ichikawa, S. Nojima and S. Yano, *Chem. Commun.*, 1999, 1181–1182.

8 S. Kutsumizu, K. Morita, T. Ichikawa, S. Yano, S. Nojima and T. Yamaguchi, *Liq. Cryst.*, 2002, **29**, 1447–1458.

9 K. Saito, T. Shinhara, T. Nakamoto, S. Kutsumizu, S. Yano and M. Sorai, *Phys. Rev. E*, 2002, **65**, 031719.

10 H. Schubert, J. Hauschild, D. Demus and S. Hoffmann, *Z. Chem.*, 1978, **18**, 256.

11 D. Demus, A. Gloza, H. Hartung, A. Hauser, I. Rapthel and A. Wiegeleben, *Cryst. Res. Technol.*, 1981, **16**, 1445–1451.

12 P. Göring, S. Diele, S. Fischer, A. Wiegeleben, G. Pelzl, H. Stegemeyer and W. Thyen, *Liq. Cryst.*, 1998, **25**, 467–474.

13 H. Mori, S. Kutsumizu, T. Ito, M. Fukatami, K. Saito, K. Sakajiri and K. Moriya, *Chem. Lett.*, 2006, **35**, 362–363.

14 S. Kutsumizu, H. Mori, M. Fukatami, S. Naito, K. Sakajiri and K. Saito, *Chem. Mater.*, 2008, **20**, 3675–3687.

15 K. Ozawa, Y. Yamamura, S. Yasuzuka, H. Mori, S. Kutsumizu and K. Saito, *J. Phys. Chem. B*, 2008, **112**, 12179–12181.

16 Y. Nakazawa, Y. Yamamura, S. Kutsumizu and K. Saito, *J. Phys. Soc. Jpn.*, 2012, **81**, 094601.

17 S. Kutsumizu, K. Morita, S. Yano and S. Nojima, *Liq. Cryst.*, 2002, **29**, 1459–1468.

18 K. Saito and M. Sorai, *Chem. Phys. Lett.*, 2002, **366**, 56–61.

19 X. Zeng, G. Ungar and M. Impéror-Clerc, *Nat. Mater.*, 2005, **4**, 562–567.

20 X. Zeng, L. Cseh, G. H. Mehl and G. Ungar, *J. Mater. Chem.*, 2008, **18**, 2953–2961.

21 D. W. Bruce, *Acc. Chem. Res.*, 2000, **33**, 831–840.

22 H.-T. Nguyen, C. Destrade and J. Malthête, in *Handbook of Liquid Crystals*, ed. D. Demus, J. Goodby, G. W. Gray, H.-W. Spiess and V. Vill, Wiley-VCH Weinheim, 1998, vol. 2B, pp. 865–885.

23 D. S. Shankar Rao, K. Krishna Prasad, V. Prasad and S. Kumar, *Phys. Rev. E*, 1999, **59**, 5572–5576.

24 Y. Maeda, G.-P. Cheng, S. Kutsumizu and S. Yano, *Liq. Cryst.*, 2001, **28**, 1785–1791.

25 Y. Maeda, S. Krishna Prasad, S. Kutsumizu and S. Yano, *Liq. Cryst.*, 2003, **30**, 7–16.

26 P. M. Duesing, J. M. Seddon, R. H. Templer and D. A. Mannock, *Langmuir*, 1997, **13**, 2655–2664.

27 R. Winter, J. Erbes, R. H. Templer, J. M. Seddon, A. Syrykh, N. A. Warrender and G. Rapp, *Phys. Chem. Chem. Phys.*, 1999, **1**, 887–893.

28 R. Winter, *Curr. Opin. Colloid Interface Sci.*, 2001, **6**, 303–312.

29 M. Pisani, S. Bernstorff, C. Ferrero and P. Mariani, *J. Phys. Chem. B*, 2001, **105**, 3109–3119.

30 L. Paccamiccio, M. Pisani, F. Spinozzi, C. Ferrero, S. Finet and P. Mariani, *J. Phys. Chem. B*, 2006, **110**, 12410–12418.

31 T.-Y. Dora Tang, N. J. Brooks, C. Jeworrek, O. Ces, N. J. Terrill, R. Winter, R. H. Templer and J. M. Seddon, *Langmuir*, 2012, **28**, 13018–13024.

32 Y. Maeda, H. Mori and S. Kutsumizu, *Liq. Cryst.*, 2010, **37**, 463–473 and references therein.

33 Y. Maeda, H. Mori and S. Kutsumizu, *Liq. Cryst.*, 2009, **36**, 217–223.

34 Y. Maeda, S. Kutsumizu and S. Sakurai, *Liq. Cryst.*, 2012, **39**, 451–455.

35 S. Sakurai and S. Kutsumizu, unpublished results.

36 K. Saito. A. Sato and M. Sorai, *Liq. Cryst.*, 1998, **25**, 525–530.

37 A. Sato, Y. Yamamura, K. Saito and M. Sorai, *Liq. Cryst.*, 1999, **26**, 1185–1195.

38 K. Saito, T. Shinhara and M. Sorai, *Liq. Cryst.*, 2000, **27**, 1555–1559.